Nanoscale

PAPER

View Article Online
View Journal | View Issue

Cite this: *Nanoscale*, 2019, **11**, 13600

Single molybdenum center supported on N-doped black phosphorus as an efficient electrocatalyst for nitrogen fixation†

Pengfei Ou,[a] Xiao Zhou,[a,b] Fanchao Meng,[a] Cheng Chen,[a] Yiqing Chen[a] and Jun Song*[a]

Ammonia (NH_3) is one of the most significant industrial chemical products due to its wide applications in various fields. However, the production of NH_3 from the electrochemical nitrogen (N_2) reduction reaction (NRR) under ambient conditions is one of the most important issues that remain challenging for chemists. Herein, the candidacy of a series of molybdenum (Mo)-based single-atom catalysts (SACs) supported on N-doped black phosphorus (BP) as the electrocatalyst for the NRR has been evaluated by means of density functional theory (DFT) calculations. In particular, Mo_1N_3 has been found to chemically adsorb N_2, and it exhibits the highest catalytic activity toward the NRR with an ultralow overpotential of 0.02 V *via* the associative distal mechanism, indicative of catalyzing the NRR under ambient conditions. Additionally, Mo_1N_3 shows the fast removal of the produced NH_3 with a free energy uphill of only 0.56 eV and good stability of NRR intermediates. Moreover, the Mo-based SACs were demonstrated to be more selective to the NRR over the competing hydrogen evolution reaction (HER) process. These excellent features render Mo_1N_3 on BP as a compelling highly efficient and durable catalyst for electrochemical N_2 fixation. Our results provide a rational paradigm for catalytic nitrogen fixation by SACs in two-dimensional (2D) materials under ambient conditions.

Received 25th March 2019,
Accepted 25th June 2019

DOI: 10.1039/c9nr02586c

rsc.li/nanoscale

1. Introduction

Synthesis of ammonia (NH_3) from naturally abundant nitrogen (N_2) is of significant importance not only for producing synthetic chemicals, such as dyes, fertilizers, medicaments, explosives, and resins,[1–4] but also for providing promising new pathways towards solving the stringent energy and environmental crisis.[5,6] Conventionally, the mass production of NH_3 mainly depends on the Haber–Bosch process, *i.e.*, a high-temperature (350–550 °C) and high-pressure (150–350 atm) reaction, which accounts for approximately 1–2% of the energy consumption worldwide.[7] Therefore, it is highly imperative to develop alternative processes that have the potential to overcome the limitations of the Haber–Bosch process.[7,8] Contrary to the industrial Haber–Bosch process, the electrochemical N_2 reduction reaction (NRR) that occurs under ambient conditions is able to significantly reduce the energy consumption and simplify the reactor design, representing a promising, attractive and alternative strategy for sustainable NH_3 production.[9] Thus, the search for an electrocatalyst that can perform electrochemical nitrogen fixation with high catalytic activity and selectivity is of paramount significance.

Recently, single-atom catalysts (SACs) have been widely explored as promising candidates for various catalytic reactions, such as the carbon dioxide (CO_2) reduction, hydrogen evolution reaction (HER), oxygen reduction reaction (ORR), carbon monoxide (CO) oxidation, NRR, *etc.*[9–28] They offer significantly improved catalytic activities and help greatly reduce the amount of noble metals used in electrocatalysts, making them much preferable than the conventional catalysts. Previous studies have suggested that drastic modifications of electronic properties of SACs from those of bulk metals can successfully manipulate the catalytic activity and selectivity.[10–14,19,23,29] Among various SACs, single molybdenum (Mo) centers within the nitrogenases (*i.e.*, Mo–N complexes) have been extensively studied, well demonstrating the significance of Mo in the design of NRR catalysts.[30–33] In 2003, Schrock and co-workers showed the catalytic reduction of N_2 to NH_3 at a single Mo center under ambient temperature and pressure in their study using Mo catalysts that contain tetra-

[a]*Department of Mining and Materials Engineering, McGill University, Montreal H3A 0C5, Canada. E-mail: jun.song2@mcgill.ca; Fax: +1 (514) 398-4492; Tel: +1 (514) 398-4592*
[b]*Institute of Mechanical Engineering, École Polytechnique Fédérale de Lausanne, Lausanne, Vaud CH-1015, Switzerland*

†Electronic supplementary information (ESI) available. See DOI: 10.1039/c9nr02586c

dentate triamidoamine ligands.[30] Later in the work by Arashiba *et al.*, Mo–N complexes bearing a mer-tridentate triphosphine as a ligand have been designed and found to be highly effective catalysts, achieving up to 63 equiv. of ammonia based on the Mo atom.[31] In a more recent study, Arashiba *et al.* further demonstrated a remarkable catalytic performance of 415 equivalent of NH_3 based on the Mo atom using Mo-iodide complexes containing a PNP-type pincer ligand.[32] In addition to the development of the yield rate, Chen *et al.* discovered a dramatically enhanced electrochemical NRR selectivity under ambient conditions *via* Li^+ incorporation into poly (*N*-ethyl-benzene-1,2,4,5-tetracarboxylic diimide) (PEBCD) as a catalyst.[34]

Inspired by the success of the design of molecular complexes, the search for Mo–N complexes for the electrochemical NRR also has been extended to other inorganic systems, particularly for two-dimensional (2D) materials.[9,21–24,35,36] Zhao *et al*. theoretically investigated the catalytic abilities of different single transition metal (TM) atoms supported on defective hexagonal boron nitride (h-BN) for nitrogen fixation and found that a single Mo atom at boron monovacancy exhibits superb catalytic activity with a low overpotential of 0.19 V.[21] Azofra *et al.* examined the Mo_3C_2 center in the 2D d^2–d^4 M_3C_2 transition metal carbides (MXenes) and demonstrated its ability to activate the chemisorbed N_2 and subsequently the catalytic conversion into NH_3.[35] Similarly, Mo_2C nanodots embedded in two-dimensional carbon nanosheets as highly efficient electrochemical NRR catalysts were first developed by Cheng *et al.*, with a high NH_3 yield rate of 11.3 μg h^{-1} mg^{-1} Mo_2C and a faradaic efficiency of 7.8%.[37] As reported by Li *et al.*, molybdenum nitride (MoN_2) nanosheet might generate N-vacancy to actively fill N_2 *via* Mo–N_3 bonding and maintain excellent performance for N_2 adsorption and activation under electrochemical conditions, especially for iron (Fe) doping.[36] More recently, Ling and co-workers computationally screened the catalytic performances of a series of single metal atoms supported on N-doped carbon by density functional theory (DFT) calculations, the authors revealed that $Mo_1N_1C_2$ can catalyze the NRR through the enzymatic mechanism under ambient conditions.[22]

Recently, the 2D counterpart of black phosphorus (BP), also known as phosphorene, has been introduced as a new member of the 2D materials family. Due to its unique physical and chemical properties, BP has already emerged as a new class of catalysts for a variety of significant reactions, such as the HER[38,39] and the oxygen evolution reaction (OER).[40,41] Very recently, Zhang *et al.* demonstrated that the well-exfoliated few-layer BP can also be implemented as a promising catalyst for the electrochemical NRR with a yield of 31.37 μg h^{-1} mg^{-1}_{cat}.[28] However, it was revealed by DFT calculations that only the edge sites can actively catalyze the electrocatalysis of N_2 to NH_3, with the rest of the basal plane inert. The outstanding properties of BP inspire us to ask: can the Mo–N complexes supported on BP be employed to further enhance the catalytic activity on the basal plane for nitrogen fixation under ambient conditions? To answer this question, we systematically investigate the catalytic performance of Mo-based SACs anchored on N-doped BP for the NRR with the help of DFT calculations. Our calculations show that Mo_1N_3 possesses ultrahigh catalytic activity for the NRR with an extremely low overpotential of 0.02 V, which ensures the efficient reduction of N_2 under ambient conditions. Surprisingly, NH_3 desorption only utilizes a free energy of 0.56 eV, leading to a rapid removal of the produced NH_3. In addition, the coordination effect on the activity and selectivity of these Mo-based SACs are further studied, and Mo_1N_3 is confirmed to possess the highest activity for the NRR. Therefore, by carefully controlling Mo doping sites, BP can be implemented as a novel noble-metal-free NRR electrocatalyst with high efficiency under ambient conditions.

2. Computational details

First-principles DFT calculations using the Vienna *Ab initio* Simulation Package (VASP)[42,43] were performed with ion–electron interactions were described by the projector-augmented wave (PAW) method.[44] The generalized gradient approximation (GGA) in the Perdew–Burke–Ernzerhof (PBE) form[45,46] and a cut-off energy of 500 eV for a plane-wave basis set were adopted. Spin-polarized calculations were employed for all systems, and the convergence criterion for the residual force was set at 0.01 eV $Å^{-1}$. The vacuum space perpendicular to the BP nanosheet was set to be larger than 15 Å, which is sufficient to avoid interactions between two periodic images. The Brillouin zone was sampled with the Monkhorst–Pack mesh with a 2 × 2 × 1 *k*-point grid.[47] The climbing-nudged elastic band method was used to locate saddle points and minimum energy paths.[48]

A 6 × 4 × 1 monolayer BP supercell containing a phosphorus single vacancy (SV) with a formation energy of 2.21 eV was used for the calculations, with the SV configuration in accordance with recent experimental characterization results using scanning tunneling microscopy/spectroscopy (STM/STS).[49] Different Mo SAC centers, in the form of $Mo_1N_iP_{3-i}$ (i = 0, 1, 2, and 3), anchored at the SV, were then created and examined. Here, i denotes the number of nitrogen atoms introduced to substitute those phosphorus atoms immediately neighboring the SV. As will be seen in the results below, the focus is placed on the Mo_1N_3 center (*i.e.*, i = 3) as it offers the best performance. Meanwhile, it is worth noting that we have also investigated Mo SAC centers anchored at a phosphorus divacancy (DV). Our results reveal that, based on the adsorption and cohesive energies, the Mo atom binds much stronger with a SV than a DV (Fig. S1 in the ESI†). Therefore, in the present study, we limit our discussion to Mo SAC centers at a phosphorus SV.

The calculations of the Gibbs free energy change (ΔG) for each elemental step were based on the computational hydrogen electrode (CHE) model proposed by Nørskov *et al.*,[50] which can be computed by the following equation:

$$\Delta G = \Delta E + \Delta E_{ZPE} - T\Delta S + eU + \Delta G_{pH} \quad (1)$$

where ΔE is the electronic energy difference before and after the adsorption of reaction intermediates, ΔE_{ZPE} and ΔS are the changes in zero-point energies and entropy, respectively. T is the temperature, set to be room temperature, *i.e.*, 298.15 K in this study. e and U are the number of electrons transferred and the applied electrode potential respectively, while ΔG_{pH} is the free energy correction of pH, calculated as $\Delta G_{pH} = k_B T \times pH \times \ln 10$. In the present study, the pH value is set at zero and thus $\Delta G_{pH} = 0$. Moreover, according to the CHE model, the overpotential (η) of the NRR process is determined to be the potential-limiting step with the most positive ΔG (ΔG_{max}), as computed by:

$$\eta = U_{equilibrium} - U_{limiting} \quad (2)$$

where $U_{equilibrium}$ is the equilibrium potential of the NRR (about −0.16 V in the present study for the reaction $N_2 + 6H^+ + 6e^- \rightarrow 2NH_3$) and $U_{limiting}$ is the applied potential required to eliminate the energy barrier of the rate-limiting step, which can be obtained by: $U_{limiting} = -\Delta G_{max}/e$. Parameter η serves as a good indicator for catalytic activity, *i.e.*, a smaller η value indicating a easier NRR process.

3. Results and discussion

3.1. Configuration and stability of Mo_1N_3

Among the various Mo SAC centers anchored at the SV, Mo_1N_3 was found to exhibit the lowest limiting potential as the NRR electrocatalyst (more details in the ESI†). Thus, here we focus on Mo_1N_3 as a representative case of the model catalysts proposed in the present study. An ultimate prerequisite for a SAC to be an effective catalyst is its good stability for long-term usage, which necessitates strong binding between the anchored atom (cluster) and the substrate material to prevent easy detachment and undesirable aggregation. The binding energy of the resultant Mo_1N_3 center at the SV is −5.25 eV or −0.63 eV with reference to an isolated Mo atom or the bulk Mo, respectively. This suggests that the Mo_1N_3 center can be stably present at the phosphorus SV. In the meantime, the kinetics of the adsorbed Mo atom to escape the SV has also been examined, showing an energy barrier of 14.6 eV for Mo to migrate from the SV site to a neighboring hollow site (see Fig. S2 in the ESI†). This extremely large barrier indicates that such a process is impossible to occur at room temperature. Fig. 1a represents the fully optimized structure of Mo_1N_3 at the SV. In the newly formed Mo_1N_3 moiety, the Mo–N bond length is 2.01 Å. Since the radius of the N atom is much smaller than that of the substituted P atom, the anchored Mo atom is inward from the monolayer BP surface by 0.76 Å.

3.2. Feasibility of Mo_1N_3 as the NRR electrocatalyst

Since N_2 is an extremely stable molecule with inert triple bonds, and the first electrochemical step of the NRR is always the hydrogenation of $*N_2$ into $*N_2H$ that breaks the strong N≡N triple bond, large energy consumption is thus inevitably needed. Therefore, the free energy change for this step ($\Delta G_{N_2-N_2H}$) is expected to stay positive, and this usually happens to be the potential-limiting step for most of the TMs regardless of the mechanism.[51] More importantly, despite the possibility of the NRR occurring *via* different mechanisms, the above step always remains the first electrochemical step. Hence, the screening efficiency will be greatly improved without losing the screening accuracy by using $\Delta G_{N_2-N_2H}$ as one of the activity descriptors. Besides, the chemisorption of N_2, which makes sufficient activation of the inert N≡N triple bond and enhances the frequency of the effective collision between reactants and catalysts. Therefore, to make sure that the limiting potential of the whole NRR process is close to or even smaller than the value of the best pure TM catalysts,[51] a general two-step strategy is suggested to be used for screening an eligible single-atom electrocatalyst for the NRR by Ling *et al.*:[24] (1) the catalyst can facilitate the chemisorption of N_2 and the hydrogenation of $*N_2$ into $*N_2H$ to warrant sufficient activation of its inert N≡N triple bond (criterion: the adsorption energy of N_2 (ΔE_{N_2}) should be more negative than −0.50 eV and the free energy barrier for the hydrogenation of $*N_2$ into $*N_2H$ ($\Delta G_{N_2-N_2H}$) should be smaller than 0.50 eV); (2) the catalyst can selectively destabilize $*NH_2$ species and achieve the fast removal of NH_3 (criterion: the free energy barrier for the hydrogenation of $*NH_2$ into $*NH_3$ ($\Delta G_{NH_2-NH_3}$) should not be more than 0.50 eV and the desorption energy of NH_3 (ΔG_{NH_3-des}) ought not to exceed 0.70 eV), to guarantee the reduction of the overpotential.

Following this screening strategy, we first computed the adsorption energies of a gas-phase N_2 molecule at Mo_1N_3 in the N-doped BP (see Fig. 1a) by considering both side-on and end-on initial adsorption configurations (see Fig. 1b and c). For the side-on configuration, both N atoms interact with the Mo atom, forming two Mo–N bonds (Fig. 1b), while for the end-on structure, only one N atom binds with the Mo atom (Fig. 1c). The calculated ΔE_{N_2} values of N_2 adsorption are −0.60 and −0.93 eV in side-on and end-on configurations respectively, both larger than −0.50 eV, indicating that N_2 can be effectively captured by the Mo_1N_3 center. Moreover, respectively for the side-on and end-on configurations, Bader charge analysis[52–55] shows that the adsorbed N_2 gains 0.53 and 0.36 e from Mo_1N_3 with the corresponding N≡N bond length elongated to 1.19 and 1.14 Å compared to that of the isolated N_2 molecule (1.11 Å). Further analysis reveals that the charge clouds are localized and distributed on both the adsorbed N_2 and Mo_1N_3 centers (Fig. S3 in the ESI†). The above results evidence the chemisorption of N_2 and indicate that the activation of the inert N≡N triple bond is possible. The calculated free energies for the hydrogenation of $*N_2$ into $*N_2H$ are with 0.31 and 0.14 eV in side-on and end-on configurations, smaller than 0.50 eV. Meanwhile, the performance of Mo_1N_3 for NH_3 generation and desorption has been examined, and it was found that the hydrogenation of $*NH_2$ and desorption of the produced $*NH_3$ would overcome energy barriers of 0.18 and 0.56 eV respectively, fulfilling the afore-mentioned screening requirements of $\Delta G_{NH_2-NH_3} < 0.5$ eV and $\Delta G_{NH_3-des} < 0.7$ eV.

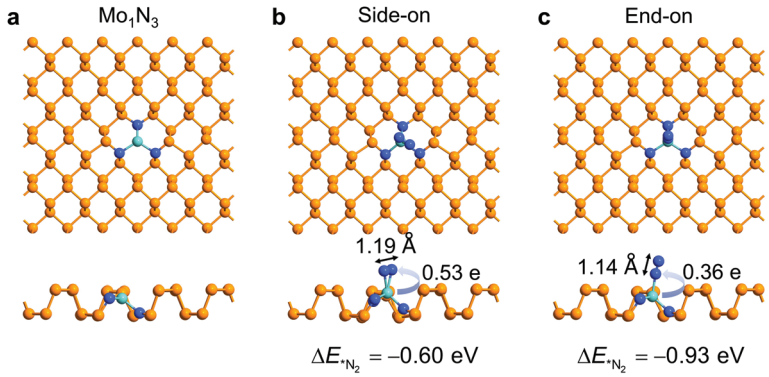

Fig. 1 Top and side views of the structures of (a) Mo_1N_3 and Mo_1N_3 with N_2 adsorption *via* (b) side-on and (c) end-on configurations. The N–N bond lengths and the corresponding amounts of charge transfer from Mo_1N_3 to N_2 are also indicated. Blue, orange, and cyan balls represent the doped N, P, and Mo atoms, respectively.

This demonstrates the ability of Mo_1N_3 of selectively destabilizing $*NH_2$ species and the rapid removal of the produced NH_3.

The above analyses confirm that the Mo_1N_3-embedded BP satisfies the criteria well in the two-step screening, and thus can serve as an eligible electrocatalyst for the NRR. In addition, to further assess the candidacy of Mo_1N_3, we have also compared it with the case of larger Mo clusters (see the ESI† for details). In general, we found that Mo_1N_3 would have superb performance compared to larger Mo clusters as the clusters exhibit weaker stabilization of $*N_2H$ species and stronger interaction with $*NH_2$ species, despite sufficient activation of the N_2 molecule (Fig. S4 in the ESI†).

3.3. Reaction mechanism and free energy for the NRR on Mo_1N_3

The NRR under electrochemical conditions is a six-electron reaction, $N_2 + 6H^+ + 6e^- \rightarrow 2NH_3$, with two potential reaction pathways, one being the dissociative pathway through which N_2 is first dissociated into two separate N atoms before being hydrogenated, and the other being the associative pathway, in which N_2 would be hydrogenated by protons simultaneously with the formation of NH_3.[51] However, the associative adsorption of N_2 is reported to be a more favorable pathway under electrochemical conditions due to the high kinetic barrier of N_2 dissociation.[56] Therefore, in the present study, we focus our investigation on the reduction processes by considering the associative pathway. According to the study by Ling *et al.*,[22] four possible reaction mechanisms are involved in the associative pathway, labeled as enzymatic and consecutive mechanisms for N_2 adsorption *via* the side-on configuration, and alternating and distal mechanisms for N_2 adsorption *via* the end-on configuration (Fig. 2 and 3). For the enzymatic and alternating mechanisms, the proton–electron pairs ($H^+ + e^-$) attack the two N atoms alternatively, whereas for the consecutive and distal mechanisms, the proton–electron pairs first attack one N atom consecutively to form a NH_3 molecule and then act on the remaining N atom to form another NH_3 molecule.

For the side-on N_2 adsorption, the corresponding structures of the NRR intermediates through enzymatic and consecutive mechanisms along with the free-energy diagrams are presented in Fig. 2 and 4a, b. From Fig. 4a and b, N_2 adsorption *via* side-on configuration exhibits a negative free energy change ΔG (−0.14 eV), indicating the ability of Mo_1N_3 to effectively capture the gas-phase N_2 molecule. We can see that the first two steps of the enzymatic and consecutive methods are essentially the same, *i.e.*, N_2 adsorption and subsequent reduction into *N–*N. However, the hydrogenation of *N–*N into *N–*NH consumes energy, with ΔG increased by 0.31 eV, being the potential-limiting step for both the enzymatic and consecutive mechanisms. Therefore, the overpotential η value for the reduction of side-on adsorbed N_2 on Mo_1N_3 becomes 0.15 V (*cf.* eqn (2)) for both enzymatic and consecutive mechanisms, indicative of overall significant efficiency.

On the other hand, for the NRR *via* the end-on configuration, Fig. 3 and Fig. 4c, d depict the free-energy diagrams and the corresponding structures of the reaction intermediates, respectively. The end-on configuration shows a more negative free energy (−0.49 eV) for N_2 adsorption than the side-on configuration, implying much stronger N_2 capture and activation. The first step is $*N_2$ hydrogenated by adsorbing a proton coupled with an electron transfer, and reduced into $*N_2H$, with the free energy slightly uphill by 0.14 eV, being smaller than that of side-on adsorbed N_2 (0.31 eV, *cf.* Fig. 4). On examining the subsequent reaction process, we found that for the distal mechanism, the potential-limiting steps are the hydrogenation of *N into *NH and $*NH_2$ into $*NH_3$, with an extremely low limiting potentials of 0.17 and 0.18 V respectively (Fig. 4d), which are much lower than that (greater than 0.50 V) from the best metal catalyst reported so far.[57] Such a low overpotential is an indication of the superior catalytic performance of Mo_1N_3 for the NRR. On the other hand, for the alternating method, the potential-limiting step is the hydrogenation of *N–*NH into *NH–*NH with a ΔG of 0.69 eV, which is the

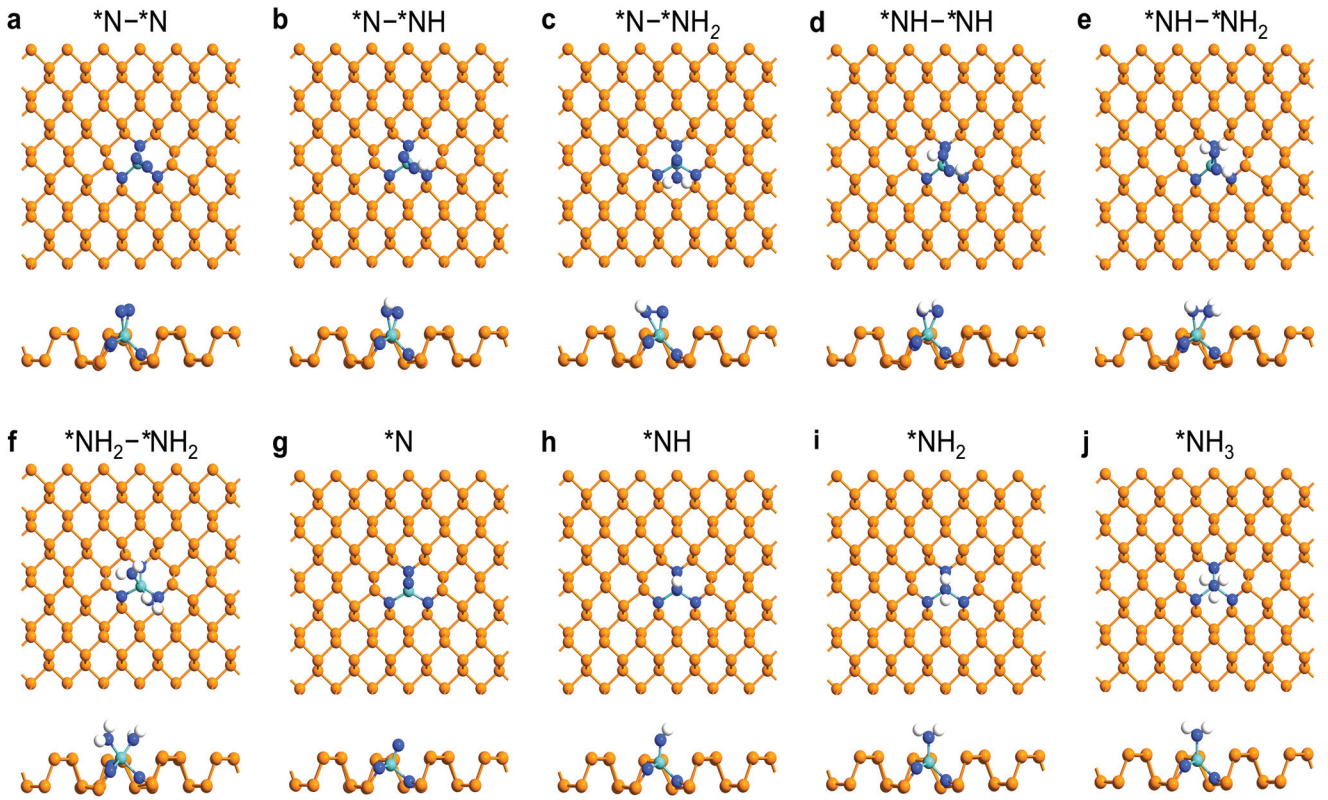

Fig. 2 The corresponding structures of the reaction intermediates through the enzymatic and consecutive mechanisms, (a) *N–*N, (b) *N–*NH, (c) *N–*NH_2, (d)*NH–*NH, (e) *NH–*NH_2, (f) *NH_2–*NH_2, (g) *N, (h) *NH, (i) NH_2, and (j) *NH_3. White, blue, orange, and cyan balls represent H, doped N, P, and Mo atoms respectively.

highest value among the four possible mechanisms, as shown in Fig. 4c. Nevertheless, despite the relatively high ΔG, the alternating mechanism exhibits an η value of 0.53 V, which is still attractive.

In the previous study by Zhang *et al.*,[28] the NRR processes on the basal plane and various edge sites (*i.e.*, armchair and zigzag edges) of BP have been thoroughly examined by DFT calculations. It is found out that the electron densities are only concentrated near the zigzag and diff-zigzag edges, which is beneficial for adsorbing N_2 and boosting the NRR performance. Moreover, they have further confirmed that the zigzag and diff-zigzag edges exhibit the lowest energy barriers of 0.85 and 0.84 eV *via* the alternating pathway in the association mechanism, respectively, with the potential-limiting step being the protonation of N_2 to N_2H. In comparison, from our present study, the energy barrier for the potential-limiting step on the Mo_1N_3 center (~0.18 eV) is significantly lower than those of the basal plane and edge sites. Therefore, the Mo_1N_3 center accounts for the major contribution to the high activity of Mo-based SACs supported on N-doped BP. Based on the above results, we see that obviously, the NRR occurring on the Mo_1N_3 in N-doped BP would prefer to proceed through the distal mechanism due to the lowest overpotential (0.02 V), which is lower than the overpotential from any catalyst previously reported for 2D materials.[9,20–24,29,58,59]

Besides the N_2 electrochemical reduction process, other factors, such as the desorption of the produced NH_3 and stability of reaction intermediates, may also play critical roles in determining the performance of the NRR catalyst.[24,56,57] Generally, to efficiently catalyze the NRR, the catalyst should have a relatively high surface activity to bind N_2 tightly enough to activate the inert N≡N triple bond sufficiently.[60] However, this high surface activity often also results in high binding strength between NH_3 and the catalyst and thus in product poisoning of the catalyst surface.[57] To this end, we examined the NH_3 desorption on Mo_1N_3, and found that despite the high binding strength between N_2 and Mo_1N_3, the ΔG value for NH_3 desorption on Mo_1N_3 is only 0.56 eV, being considerably lower than those of the recently reported candidates for highly active catalysts for the NRR, *e.g.*, V_3C_2, Nb_3C_2, and single Mo center on defective BN, which exhibit high ΔG values of 0.92, 1.16, and 0.70 eV, respectively.[21,35] This indicates a much faster removal of the produced NH_3 molecule from Mo_1N_3 and thus better durability of the catalyst. Meanwhile, for the stability of reaction intermediates, we considered the possibility of hydrazine (N_2H_4) production in the enzymatic and alternating mechanisms. The release of N_2H_4 is found to require energies of ~2.35 and 1.15 eV in enzymatic and alternating mechanisms respectively, which are significantly larger than that of the hydrogenation of *NH_2–*NH_2

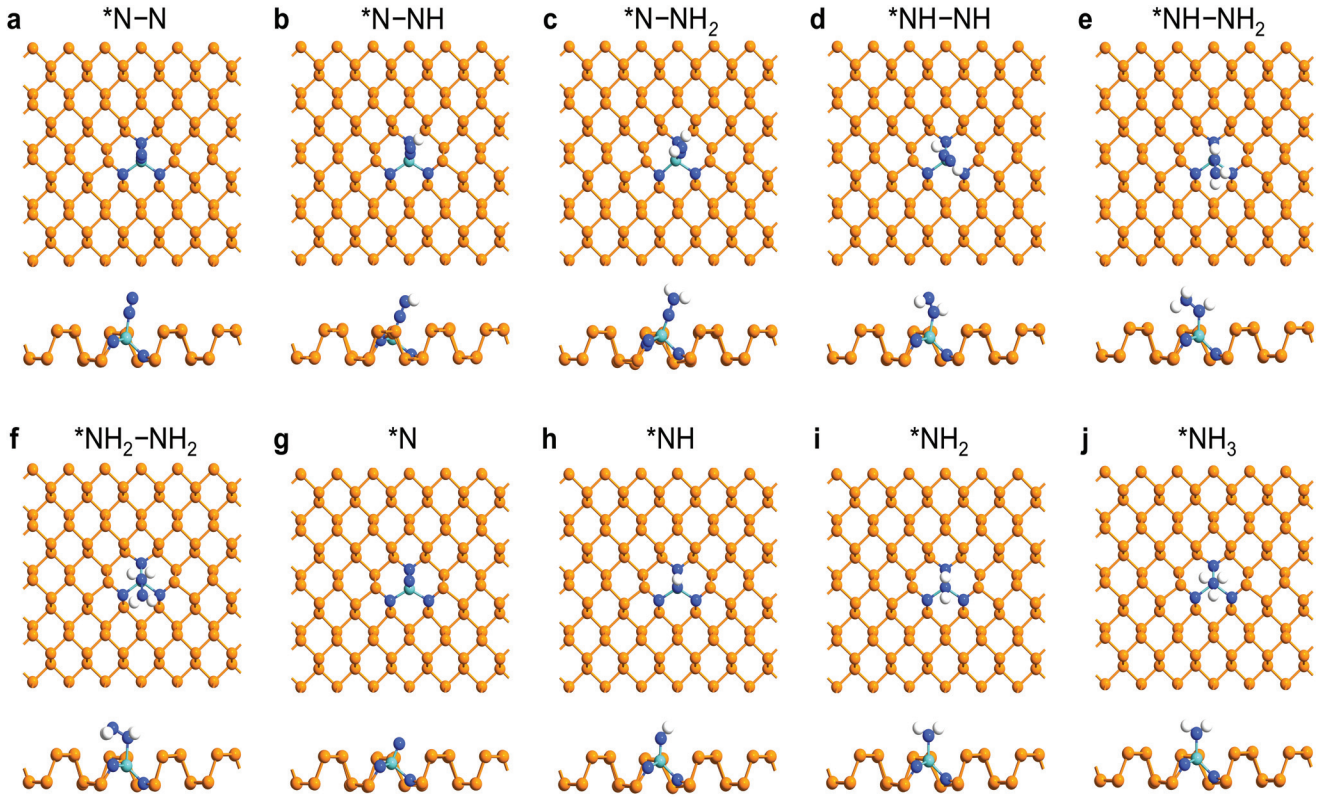

Fig. 3 The corresponding structures of the reaction intermediates through the alternating and distal mechanisms, (a) *N–N, (b) *N–NH, (c) *N–NH_2, (d)*NH–NH, (e) *NH–NH_2, (f) *NH_2–NH_2, (g) *N, (h) *NH, (i) *NH_2, and (j) *NH_3. White, blue, orange, and cyan balls represent H, doped N, P, and Mo atoms, respectively.

into *NH_2–*NH_3 in enzymatic mechanism (−0.54 eV) and the release of first NH_3 in alternating mechanism (−2.13 eV), implying that this process would not occur at room temperature.

Moreover, to gain more insights into the excellent electrocatalytic performance of Mo_1N_3, we investigated the charge variation during the NRR process. According to previous studies, each intermediate can be divided into three moieties (as shown in Fig. 5a), including moiety 1 (BP without Mo_1N_3), moiety 2 (Mo_1N_3 center), and moiety 3 (the adsorbed *N_xH_y species).[20–22] Fig. 5b shows the charge variations in each elementary reaction step, considering the distal mechanism as the representative. The charge variation here is defined as the charge difference of each moiety between the present step and the previous step, which is calculated using the Bader charge analysis.[52–55] The charge transfer occurs only between Mo_1N_3 and *N_xH_y species in the first three steps, as the charge variation of the BP moiety is close to 0. As shown in Fig. 5b, N_2 gains 0.36 e when adsorbed onto Mo_1N_3, where the charge is mainly donated by moiety 2, similarly for the hydrogenation of *N_2 into *N–NH. However, the electrons are transferred from the adsorbed *N_xH_y species to Mo_1N_3 when *N–NH is hydrogenated to *N–NH_2. In contrast, the BP moiety will actively participate in transferring electrons between Mo_1N_3 and N_xH_y species in the subsequent four hydrogenation processes, which facilitates the formation and removal of the second NH_3 molecule. Besides, N–N bond lengths in each intermediate along the pathway (Fig. 5c) increase monotonously, indicative of the gradual activation process of N_2. Moreover, from gas phase N_2 to *N–*NH_2 (where the N–N has not been broken), the N–N bond length presents a nearly linear increase, implying that the stretching effect of adsorption is comparable to that of the hydrogenation.

3.4. Doping effect of SACs

Our discussion above focused on the Mo_1N_3 center as a representative. Nonetheless, in practice, the Mo SAC center may assume a general form (*i.e.*, $Mo_1N_iP_{3-i}$ (i = 0, 1, 2, or 3)), thus giving rise of varying NRR performances.[30,31,61] Therefore, it is important to investigate the doping effect on the performance of the Mo SAC center ($Mo_1N_iP_{3-i}$) as i varies. In this regard, other types of active centers, *i.e.*, symmetric (*sym_*) and asymmetric (*asym_*) $Mo_1N_2P_1$ and $Mo_1N_1P_2$, as well as Mo_1P_3, have been constructed (as shown in Fig. 6a–e), with their performance in the NRR process has been evaluated, and the corresponding free energy diagrams for the reduction of N_2 to NH_3 at zero and applied potentials calculated, summarized in Fig. S5–S9 (see the ESI†).

Like the case of Mo_1N_3, for all those Mo SACs, the end-on adsorption of N_2 is more energetically favorable than the side-

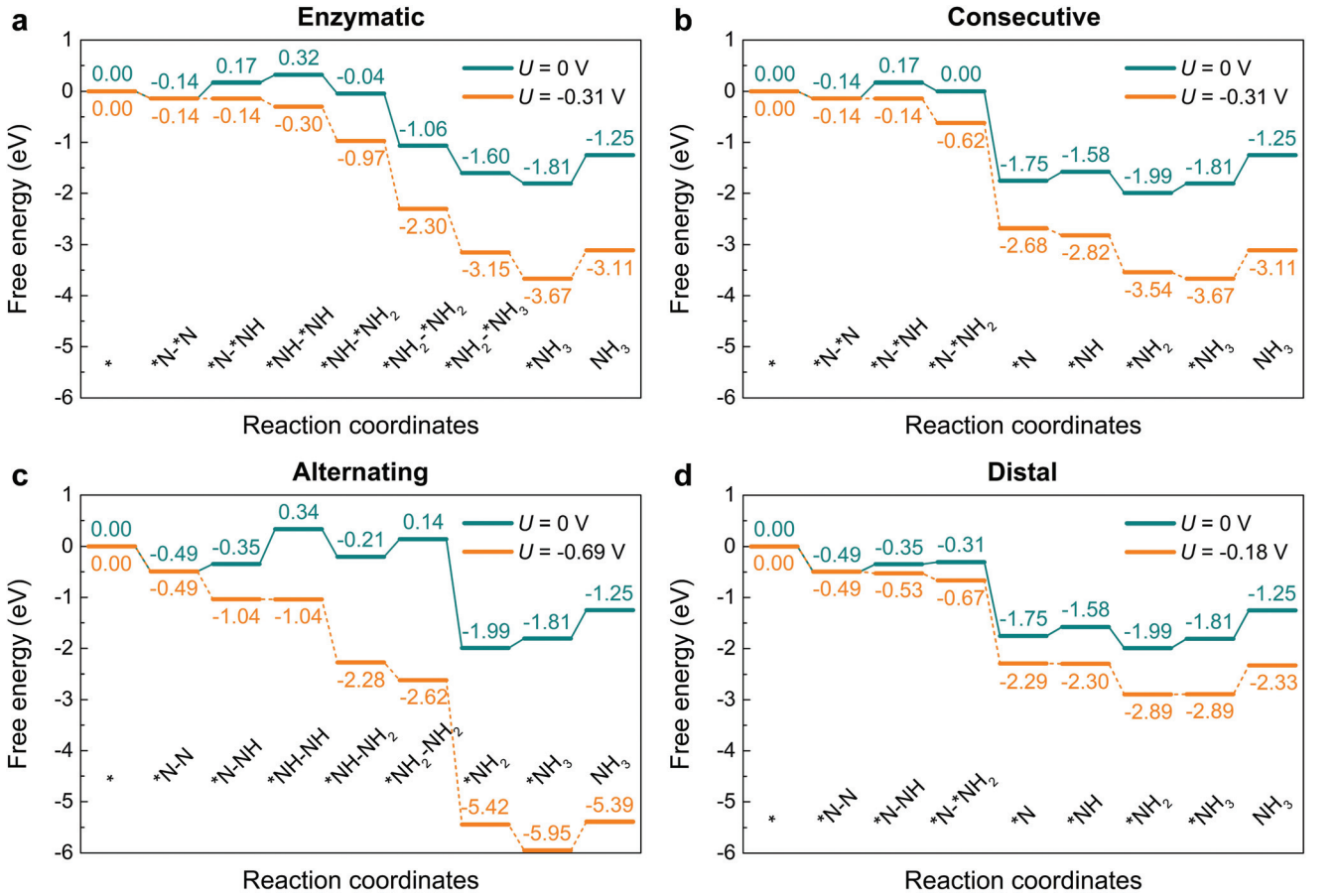

Fig. 4 Free energy diagrams of the reduction of N_2 to NH_3 through (a) enzymatic, (b) consecutive, (c) alternating, and (d) distal mechanisms on Mo_1N_3 at zero and applied potentials. The green and orange curves respectively correspond to the free energy changes for NRR at 0 V and limiting potentials *versus* RHE, respectively.

on adsorption (see the ESI†). However, unlike Mo_1N_3, several Mo SACs (*i.e.*, *sym*_$Mo_1N_2P_1$ and $Mo_1N_1P_2$, and Mo_1P_3, see the ESI†) would catalyze the NRR through the enzymatic mechanism other than the distal mechanism, despite the more energetically favored end-on adsorption of N_2. From the calculation results, the limiting potentials are determined to be 0.45 (Mo_1P_3), 0.33 ($Mo_1N_1P_2$, averaged from the symmetric and asymmetric configurations), 0.28 ($Mo_1N_2P_1$, averaged from the symmetric and asymmetric configurations), and 0.18 V (Mo_1N_3). We see that the limiting potential monotonously decreases with an increasing number of coordinated N atoms. Moreover, it was found that unlike Mo_1N_3 for which the hydrogenation of $*NH_2$ to $*NH_3$ is the potential-limiting step, $Mo_1N_2P_1$, $Mo_1N_1P_2$, and Mo_1P_3 all have the hydrogenation of $*N_2$ into $*NH_2$ as the potential-limiting step. Generally, the chemisorption of the N_2 gas phase onto the surface of the catalysts is the prerequisite for an efficient NRR process. For TM-based catalysts, their strong binding strength with N_2 can be ascribed to their advantageous combination of empty and occupied d orbitals. On the one hand, due to the existence of lone-pair electrons of N_2, TM centers need to have empty d orbitals to accept the lone-pair electrons. On the other hand, to enhance the N–TM bonds, the TM atoms should have separate d electrons that can be donated into the anti-binding orbital and weaken the N≡N triple bond. Therefore, "acceptance–donation" of electrons is the nature of the interaction between the TM and N_2, where the combination of empty and occupied d orbitals plays a key role.[62] In the case of Mo-based SACs, the electronic configuration of the Mo atom is $4d^5 5s^1$, and the sp^3d^2 hybridization of these orbitals will result in six half occupied orbitals and no empty orbitals. Therefore, the surrounding N atom acts as an electron acceptor due to its strong electronegativity to guarantee that the Mo atom has the empty d orbitals to accept the lone-pair electrons from N_2. This is also evidenced by the calculations of the doping effect on the NRR limiting potential, that is, the limiting potential monotonously decreases with an increasing number of coordinated N atoms.

From the above results, we see that the Mo SAC group (*i.e.*, $Mo_1N_iP_{3-i}$) generally exhibits good performance in catalyzing the NRR, yet the effectiveness is much dependent on the number of coordinated N atoms, with Mo_1N_3 possessing sites of the highest activity with an ultralow overpotential of 0.02 eV.

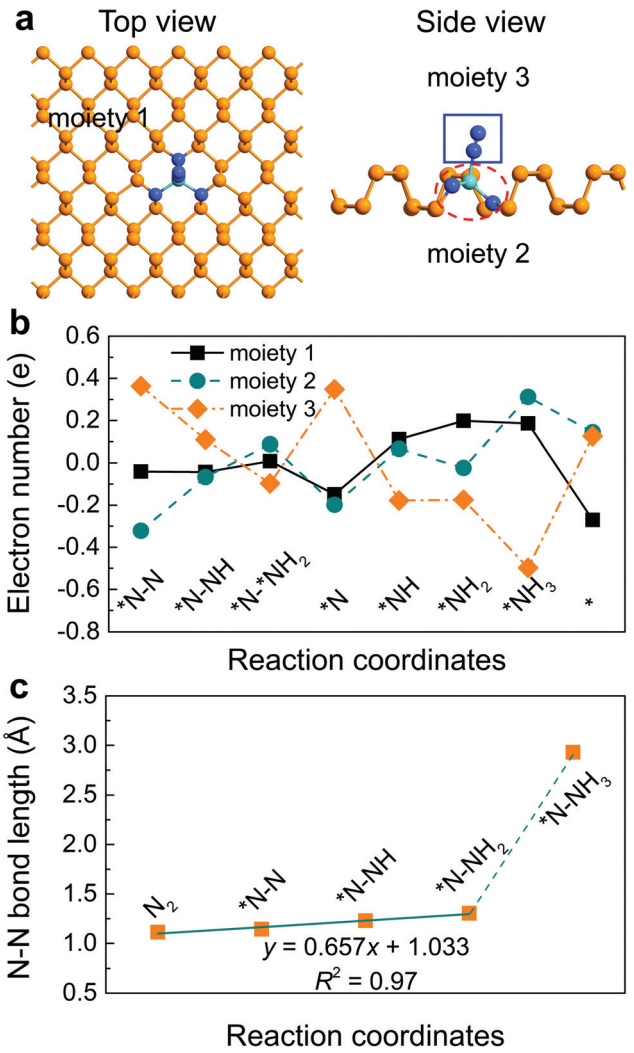

Fig. 5 (a) Top and side views of three moieties, *i.e.*, moiety 1 (BP without Mo_1N_3), moiety 2 (the Mo_1N_3 center), and moiety 3 (the adsorbed $*N_xH_y$ species), of the *N–N intermediate. (b) Charge variation of the three moieties. (c) The N–N bond length at different reaction coordinates along the distal mechanism *via* end-on adsorption, where the bond length is observed to increase linearly before the final bond breakage.

3.5. Competition with the hydrogen evolution reaction

As mentioned above, the free energy diagram for the NRR on Mo_1N_3 demonstrated its superior electrocatalytic activity, which well surpasses those of the previously reported SACs in 2D materials.[9,20–24,29,58,59] As the required proton for the NRR is provided by the aqueous solution in the electrochemical environments, the H adsorption will be thermodynamically more favored than the N_2 adsorption with negative potentials.[51,56] Therefore, the catalyst surface is easily covered by *H, and consequently such coverage would result in the blockage of active sites for the NRR to seriously reduce the faradaic efficiency.[8,63–66] Thus, in efforts to enhance the NRR selectivity, the suppression of hydrogen adsorption is also an important factor to consider.[67,68] In this regard, we investigated hydrogen adsorption related to the HER. Specifically, we investigated the selectivity of the NRR over the HER on different Mo SACs in BP by considering $*N_2$/*H selectivity. This can be quantitatively assessed by examining the free energy changes of the first reaction step for these two reactions, namely ΔG_{*N_2} and ΔG_{*H} (N_2 and H adsorption for the NRR and HER, respectively), where a reaction with lower free energy is assumed to be more selective.[69] The results are illustrated in Fig. 6g, where the catalysts in the upper left corner and lower right corner are the HER and NRR dominant, respectively. We can clearly see that for all the Mo SACs considered, the NRR is preferred over the HER. The selective electrocatalysis of N_2 to NH_3 on SACs can be largely attributed to the great suppression of the HER with the synergy of geometric and electronic effects, which has been observed in previous studies on SACs in other systems, such as defective graphene[23] and $Ti_3C_2T_x$ MXene.[70] For the geometric effect, at a SAC, a single metal atom exists at the active site and thus only the top site adsorption is possible on a SAC, whereas there are many metal atoms in the bulk metal surface and several adsorption sites (bridge and hollow sites) are available. On the metal surface, *H prefers bridge and hollow sites to a top site, and *H can be destabilized on the top site. Therefore, the suppressed H adsorption thus originates from the availability of only the top adsorption sites on SACs, meaning that the atomic ensemble effect can play an important role in suppressing the HER. In terms of the electronic effect, the electronic structures of SACs are quite different from those of bulk metals due to strong metal–support interaction.[17] It can lead to charge transfer between metal and support; thus an anchored metal atom usually carries some positive charge.[10,17] Consequently, the electronic structure of a SAC would benefit the N_2 adsorption ability of the metal. This is also evidenced by the calculated spin-resolved density states of N_2-adsorbed Mo_1N_3, as shown in Fig. S3 in the ESI.† It is shown that the negative charges are localized and distributed on the adsorbed N_2, while the positive charges around the anchored Mo atom.

In order to further enhance the selectivity in the design of a catalyst, other possible methods are also proposed and discussed in the previous studies.[34,71] For instance, one method is the ion incorporation strategy, in which the Li^+ ions are incorporated into poly(*N*-ethyl-benzene-1,2,4,5-tetracarboxylic diimide) (PEBCD) to either hinder the Tafel or the Heyrovsky reaction, which results in high selectivity for the NRR.[34] Another possible method is to use a hydrophobic protection layer surrounding the catalyst to overcome HER-imposed bottlenecks due to its water-repelling and molecular-concentrating effects.[71] More specifically, Ling and co-workers achieved excellent NRR selectivity of ~90% under ambient conditions by coating a superhydrophobic metal–organic framework (MOF) layer over the Ag–Au platform as the NRR electrocatalyst.[71]

Further from Fig. 6g, we note that despite the selectivity of the NRR over the HER for those Mo SACs, the calculated ΔG_{*H} values are within the range of ± 0.3 eV (the optimal catalytic activity appears for ΔG_{*H} = 0 eV in terms of the HER). Given

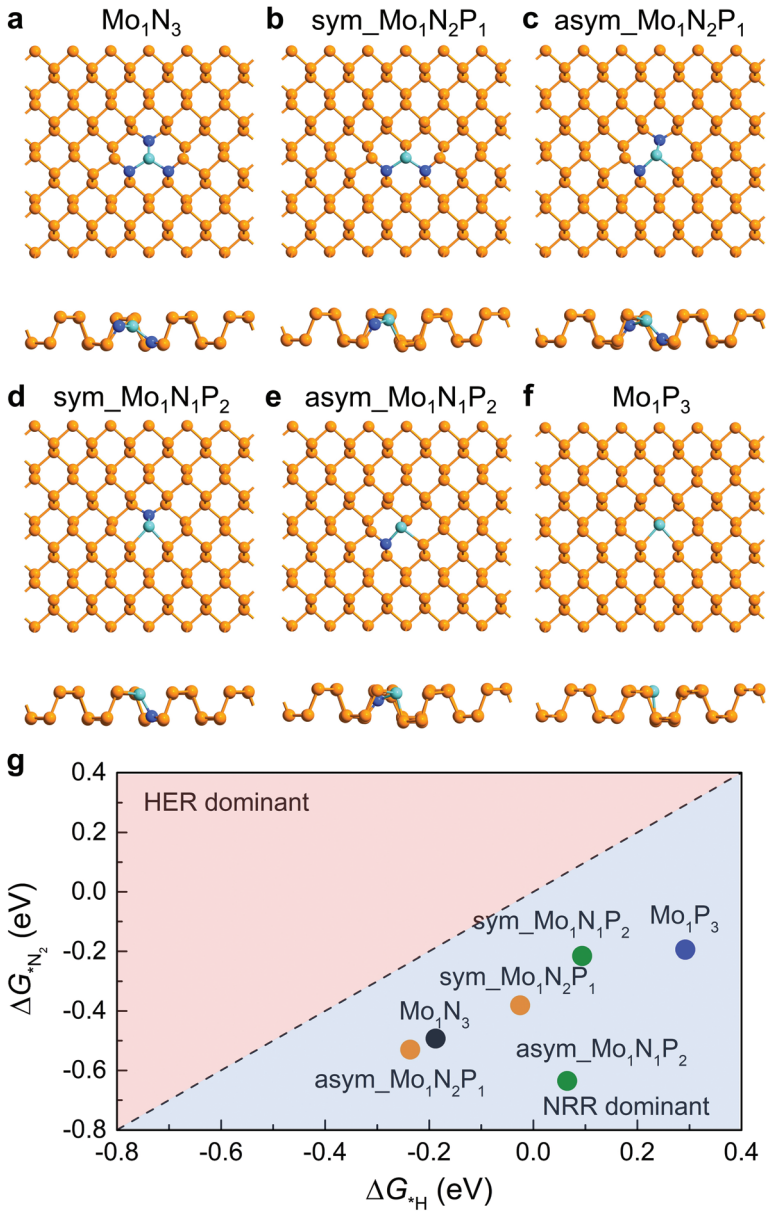

Fig. 6 Top and side views of the optimized configurations for (a) Mo_1N_3, (b) *sym*_$Mo_1N_2P_1$, (c) *asym*_$Mo_1N_2P_1$, (d) *sym*_$Mo_1N_1P_2$, (e) *asym*_$Mo_1N_1P_2$, and (f) Mo_1P_3 SACs. (g) Calculated free energies for hydrogen (ΔG_{*H}) and N_2 adsorption (ΔG_{*N_2}) of all SACs. The red and blue shaded regions in (g) respectively correspond to the HER dominant ($\Delta G_{*H} < \Delta G_{*N_2}$) and NRR dominant ($\Delta G_{*H} > \Delta G_{*N_2}$) regions at 0 V *versus* RHE.

that the top-line HER catalysts (such as Pt or Pt-based catalysts) show that $|\Delta G_{*H}| < 0.1$ eV,[57,72,73] it is also significant to note that the current SAC candidates can also be used for other electrocatalytic reactions that require the careful control of ΔG_{*H} (*e.g.*, catalysts for the HER itself).

4. Conclusions

In summary, we have systematically investigated the potential of Mo-based SACs embedded in N-doped BP for the electrochemical reduction of N_2 into NH_3. Among those Mo-based SACs considered, Mo_1N_3 has been found to exhibit the chemisorption of N_2, and an extremely low overpotential of just 0.02 V through the associative distal mechanism, indicative of catalyzing the NRR under ambient conditions. In addition, Mo_1N_3 shows the fast removal of the produced NH_3 molecule with a small free energy barrier of 0.56 eV that is lower than most of the reported NRR catalysts with low overpotential, and good stability of NRR reaction intermediates. Moreover, the Mo-based SACs were demonstrated to be more selective to the NRR over the competing HER process. These excellent features render Mo_1N_3 on BP as a compelling highly efficient and durable catalyst for electrochemical N_2 fixation. Our findings

also further demonstrated the great potential of 2D materials and might contribute to motivating more experimental and theoretical efforts targeting the usage of 2D materials in NRR electrocatalysts.

Conflicts of interest

The authors declare no competing financial interest.

Acknowledgements

This research is supported by the NSERC Discovery grant (grant # RGPIN-2017-05187), the NSERC Strategic grant (grant # STPGP 494012-16), and the McGill Engineering Doctoral Award (MEDA). The authors also would like to acknowledge the Supercomputer Consortium Laval UQAM McGill and Eastern Quebec for providing computing resources.

References

1 J. W. Erisman, M. A. Sutton, J. Galloway, Z. Klimont and W. Winiwarter, How a Century of Ammonia Synthesis Changed the World, *Nat. Geosci.*, 2008, **1**, 636.
2 R. Schlögl, Catalytic Synthesis of Ammonia—a "Never-Ending Story"?, *Angew. Chem., Int. Ed.*, 2003, **42**, 2004–2008.
3 J. N. Galloway, A. R. Townsend, J. W. Erisman, M. Bekunda, Z. Cai, J. R. Freney, L. A. Martinelli, S. P. Seitzinger and M. A. Sutton, Transformation of the Nitrogen Cycle: Recent Trends, Questions, and Potential Solutions, *Science*, 2008, **320**, 889–892.
4 D. E. Canfield, A. N. Glazer and P. G. Falkowski, The Evolution and Future of Earth's Nitrogen Cycle, *Science*, 2010, **330**, 192–196.
5 J. G. Chen, R. M. Crooks, L. C. Seefeldt, K. L. Bren, R. M. Bullock, M. Y. Darensbourg, P. L. Holland, B. Hoffman, M. J. Janik and A. K. Jones, Beyond Fossil Fuel–Driven Nitrogen Transformations, *Science*, 2018, **360**, eaar6611.
6 P. Chen, Across the Board: Ping Chen, *ChemSusChem*, 2018, **11**, 2469–2471.
7 C. J. Van der Ham, M. T. Koper and D. G. Hetterscheid, Challenges in Reduction of Dinitrogen by Proton and Electron Transfer, *Chem. Soc. Rev.*, 2014, **43**, 5183–5191.
8 M. M. Shi, D. Bao, B. R. Wulan, Y. H. Li, Y. F. Zhang, J. M. Yan and Q. Jiang, Au Sub-Nanoclusters on TiO_2 toward Highly Efficient and Selective Electrocatalyst for N_2 Conversion to Nh_3 at Ambient Conditions, *Adv. Mater.*, 2017, **29**, 1606550.
9 Z. Chen, J. Zhao, C. R. Cabrera and Z. Chen, Computational Screening of Efficient Single-Atom Catalysts Based on Graphitic Carbon Nitride (G-C_3N_4) for Nitrogen Electroreduction, *Small Methods*, 2018, 1800368.
10 S. Back, J. Lim, N.-Y. Kim, Y.-H. Kim and Y. Jung, Single-Atom Catalysts for CO_2 Electroreduction with Significant Activity and Selectivity Improvements, *Chem. Sci.*, 2017, **8**, 1090–1096.
11 M.-J. Cheng, Y. Kwon, M. Head-Gordon and A. T. Bell, Tailoring Metal-Porphyrin-Like Active Sites on Graphene to Improve the Efficiency and Selectivity of Electrochemical Co2 Reduction, *J. Phys. Chem. C*, 2015, **119**, 21345–21352.
12 N. Kornienko, Y. Zhao, C. S. Kley, C. Zhu, D. Kim, S. Lin, C. J. Chang, O. M. Yaghi and P. Yang, Metal–Organic Frameworks for Electrocatalytic Reduction of Carbon Dioxide, *J. Am. Chem. Soc.*, 2015, **137**, 14129–14135.
13 S. Lin, C. S. Diercks, Y.-B. Zhang, N. Kornienko, E. M. Nichols, Y. Zhao, A. R. Paris, D. Kim, P. Yang and O. M. Yaghi, Covalent Organic Frameworks Comprising Cobalt Porphyrins for Catalytic CO_2 Reduction in Water, *Science*, 2015, **349**, 1208–1213.
14 Z. Weng, J. Jiang, Y. Wu, Z. Wu, X. Guo, K. L. Materna, W. Liu, V. S. Batista, G. W. Brudvig and H. Wang, Electrochemical CO_2 Reduction to Hydrocarbons on a Heterogeneous Molecular Cu Catalyst in Aqueous Solution, *J. Am. Chem. Soc.*, 2016, **138**, 8076–8079.
15 B. Qiao, A. Wang, X. Yang, L. F. Allard, Z. Jiang, Y. Cui, J. Liu, J. Li and T. Zhang, Single-Atom Catalysis of Co Oxidation Using Pt_1/FeO_x, *Nat. Chem.*, 2011, **3**, 634.
16 H. J. Qiu, Y. Ito, W. Cong, Y. Tan, P. Liu, A. Hirata, T. Fujita, Z. Tang and M. Chen, Nanoporous Graphene with Single-Atom Nickel Dopants: An Efficient and Stable Catalyst for Electrochemical Hydrogen Production, *Angew. Chem., Int. Ed.*, 2015, **54**, 14031–14035.
17 X.-F. Yang, A. Wang, B. Qiao, J. Li, J. Liu and T. Zhang, Single-Atom Catalysts: A New Frontier in Heterogeneous Catalysis, *Acc. Chem. Res.*, 2013, **46**, 1740–1748.
18 S. Yang, J. Kim, Y. J. Tak, A. Soon and H. Lee, Single-Atom Catalyst of Platinum Supported on Titanium Nitride for Selective Electrochemical Reactions, *Angew. Chem., Int. Ed.*, 2016, **55**, 2058–2062.
19 D. H. Lee, W. J. Lee, W. J. Lee, S. O. Kim and Y.-H. Kim, Theory, Synthesis, and Oxygen Reduction Catalysis of Fe-Porphyrin-Like Carbon Nanotube, *Phys. Rev. Lett.*, 2011, **106**, 175502.
20 X.-F. Li, Q.-K. Li, J. Cheng, L. Liu, Q. Yan, Y. Wu, X.-H. Zhang, Z.-Y. Wang, Q. Qiu and Y. Luo, Conversion of Dinitrogen to Ammonia by FeN_3-Embedded Graphene, *J. Am. Chem. Soc.*, 2016, **138**, 8706–8709.
21 J. Zhao and Z. Chen, Single Mo Atom Supported on Defective Boron Nitride Monolayer as an Efficient Electrocatalyst for Nitrogen Fixation: A Computational Study, *J. Am. Chem. Soc.*, 2017, **139**, 12480–12487.
22 C. Ling, X. Bai, Y. Ouyang, A. Du and J. Wang, Single Molybdenum Atom Anchored on N-Doped Carbon as a Promising Electrocatalyst for Nitrogen Reduction into Ammonia at Ambient Conditions, *J. Phys. Chem. C*, 2018, **122**, 16842–16847.
23 C. Choi, S. Back, N.-Y. Kim, J. Lim, Y.-H. Kim and Y. Jung, Suppression of Hydrogen Evolution Reaction in

Electrochemical N_2 Reduction Using Single-Atom Catalysts: A Computational Guideline, *ACS Catal.*, 2018, **8**, 7517–7525.

24 C. Ling, Y. Ouyang, Q. Li, X. Bai, X. Mao, A. Du and J. Wang, A General Two-Step Strategy–Based High-Throughput Screening of Single Atom Catalysts for Nitrogen Fixation, *Small Methods*, 2018, 1800376.

25 S. Li, P. Tuo, J. Xie, X. Zhang, J. Xu, J. Bao, B. Pan and Y. Xie, Ultrathin MXene Nanosheets with Rich Fluorine Termination Groups Realizing Efficient Electrocatalytic Hydrogen Evolution, *Nano Energy*, 2018, **47**, 512–518.

26 J. Xie and Y. Xie, Transition Metal Nitrides for Electrocatalytic Energy Conversion: Opportunities and Challenges, *Chem. – Eur. J.*, 2016, **22**, 3588–3598.

27 K. Xu, P. Chen, X. Li, Y. Tong, H. Ding, X. Wu, W. Chu, Z. Peng, C. Wu and Y. Xie, Metallic Nickel Nitride Nanosheets Realizing Enhanced Electrochemical Water Oxidation, *J. Am. Chem. Soc.*, 2015, **137**, 4119–4125.

28 L. Zhang, L. X. Ding, G. F. Chen, X. Yang and H. Wang, Ammonia Synthesis under Ambient Conditions: Selective Electroreduction of Dinitrogen to Ammonia on Black Phosphorus Nanosheets, *Angew. Chem.*, 2019, **58**, 2612–2616.

29 X. Li, W. Zhong, P. Cui, J. Li and J. Jiang, Design of Efficient Catalysts with Double Transition Metal Atoms on C_2N Layer, *J. Phys. Chem. Lett.*, 2016, **7**, 1750–1755.

30 D. V. Yandulov and R. R. Schrock, Catalytic Reduction of Dinitrogen to Ammonia at a Single Molybdenum Center, *Science*, 2003, **301**, 76–78.

31 K. Arashiba, E. Kinoshita, S. Kuriyama, A. Eizawa, K. Nakajima, H. Tanaka, K. Yoshizawa and Y. Nishibayashi, Catalytic Reduction of Dinitrogen to Ammonia by Use of Molybdenum–Nitride Complexes Bearing a Tridentate Triphosphine as Catalysts, *J. Am. Chem. Soc.*, 2015, **137**, 5666–5669.

32 K. Arashiba, A. Eizawa, H. Tanaka, K. Nakajima, K. Yoshizawa and Y. Nishibayashi, Catalytic Nitrogen Fixation Via Direct Cleavage of Nitrogen–Nitrogen Triple Bond of Molecular Dinitrogen under Ambient Reaction Conditions, *Bull. Chem. Soc. Jpn.*, 2017, **90**, 1111–1118.

33 A. Eizawa, K. Arashiba, H. Tanaka, S. Kuriyama, Y. Matsuo, K. Nakajima, K. Yoshizawa and Y. Nishibayashi, Remarkable Catalytic Activity of Dinitrogen-Bridged Dimolybdenum Complexes Bearing NHC-Based PCP-Pincer Ligands toward Nitrogen Fixation, *Nat. Commun.*, 2017, **8**, 14874.

34 G. F. Chen, X. Cao, S. Wu, X. Zeng, L. X. Ding, M. Zhu and H. Wang, Ammonia Electrosynthesis with High Selectivity under Ambient Conditions Via a Li^+ Incorporation Strategy, *J. Am. Chem. Soc.*, 2017, **139**, 9771–9774.

35 L. M. Azofra, N. Li, D. R. MacFarlane and C. Sun, Promising Prospects for 2D D^2–D^4 M_3C_2 Transition Metal Carbides (Mxenes) in N_2 Capture and Conversion into Ammonia, *Energy Environ. Sci.*, 2016, **9**, 2545–2549.

36 Q. Li, L. He, C. Sun and X. Zhang, Computational Study of Mon_2 Monolayer as Electrochemical Catalysts for Nitrogen Reduction, *J. Phys. Chem. C*, 2017, **121**, 27563–27568.

37 H. Cheng, L. X. Ding, G. F. Chen, L. Zhang, J. Xue and H. Wang, Molybdenum Carbide Nanodots Enable Efficient Electrocatalytic Nitrogen Fixation under Ambient Conditions, *Adv. Mater.*, 2018, **30**, e1803694.

38 M. Zhu, S. Kim, L. Mao, M. Fujitsuka, J. Zhang, X. Wang and T. Majima, Metal-Free Photocatalyst for H_2 Evolution in Visible to near-Infrared Region: Black Phosphorus/Graphitic Carbon Nitride, *J. Am. Chem. Soc.*, 2017, **139**, 13234–13242.

39 M. Zhu, Y. Osakada, S. Kim, M. Fujitsuka and T. Majima, Black Phosphorus: A Promising Two Dimensional Visible and near-Infrared-Activated Photocatalyst for Hydrogen Evolution, *Appl. Catal., B*, 2017, **217**, 285–292.

40 Q. Jiang, L. Xu, N. Chen, H. Zhang, L. Dai and S. Wang, Facile Synthesis of Black Phosphorus: An Efficient Electrocatalyst for the Oxygen Evolving Reaction, *Angew. Chem., Int. Ed.*, 2016, **55**, 13849–13853.

41 X. Ren, J. Zhou, X. Qi, Y. Liu, Z. Huang, Z. Li, Y. Ge, S. C. Dhanabalan, J. S. Ponraj and S. Wang, Few-Layer Black Phosphorus Nanosheets as Electrocatalysts for Highly Efficient Oxygen Evolution Reaction, *Adv. Energy Mater.*, 2017, **7**, 1700396.

42 G. Kresse and J. Furthmüller, Efficient Iterative Schemes for Ab Initio Total-Energy Calculations Using a Plane-Wave Basis Set, *Phys. Rev. B: Condens. Matter Mater. Phys.*, 1996, **54**, 11169.

43 G. Kresse and D. Joubert, From Ultrasoft Pseudopotentials to the Projector Augmented-Wave Method, *Phys. Rev. B: Condens. Matter Mater. Phys.*, 1999, **59**, 1758.

44 P. E. Blöchl, Projector Augmented-Wave Method, *Phys. Rev. B: Condens. Matter Mater. Phys.*, 1994, **50**, 17953.

45 J. P. Perdew, J. A. Chevary, S. H. Vosko, K. A. Jackson, M. R. Pederson, D. J. Singh and C. Fiolhais, Atoms, Molecules, Solids, and Surfaces: Applications of the Generalized Gradient Approximation for Exchange and Correlation, *Phys. Rev. B: Condens. Matter Mater. Phys.*, 1992, **46**, 6671.

46 J. P. Perdew and Y. Wang, Accurate and Simple Analytic Representation of the Electron-Gas Correlation Energy, *Phys. Rev. B: Condens. Matter Mater. Phys.*, 1992, **45**, 13244.

47 H. J. Monkhorst and J. D. Pack, Special Points for Brillouin-Zone Integrations, *Phys. Rev. B: Solid State*, 1976, **13**, 5188.

48 G. Henkelman, B. P. Uberuaga and H. Jónsson, A Climbing Image Nudged Elastic Band Method for Finding Saddle Points and Minimum Energy Paths, *J. Chem. Phys.*, 2000, **113**, 9901–9904.

49 Y. Guo and J. Robertson, Vacancy and Doping States in Monolayer and Bulk Black Phosphorus, *Sci. Rep.*, 2015, **5**, 14165.

50 A. A. Peterson, F. Abild-Pedersen, F. Studt, J. Rossmeisl and J. K. Nørskov, How Copper Catalyzes the Electroreduction of Carbon Dioxide into Hydrocarbon Fuels, *Energy Environ. Sci.*, 2010, **3**, 1311–1315.

51 E. Skulason, T. Bligaard, S. Gudmundsdóttir, F. Studt, J. Rossmeisl, F. Abild-Pedersen, T. Vegge, H. Jónsson and

J. K. Nørskov, A Theoretical Evaluation of Possible Transition Metal Electro-Catalysts for N_2 Reduction, *Phys. Chem. Chem. Phys.*, 2012, **14**, 1235–1245.

52 G. Henkelman, A. Arnaldsson and H. Jónsson, A Fast and Robust Algorithm for Bader Decomposition of Charge Density, *Comput. Mater. Sci.*, 2006, **36**, 354–360.

53 E. Sanville, S. D. Kenny, R. Smith and G. Henkelman, Improved Grid-Based Algorithm for Bader Charge Allocation, *J. Comput. Chem.*, 2007, **28**, 899–908.

54 W. Tang, E. Sanville and G. Henkelman, A Grid-Based Bader Analysis Algorithm without Lattice Bias, *J. Phys.: Condens. Matter*, 2009, **21**, 084204.

55 M. Yu and D. R. Trinkle, Accurate and Efficient Algorithm for Bader Charge Integration, *J. Chem. Phys.*, 2011, **134**, 064111.

56 J. H. Montoya, C. Tsai, A. Vojvodic and J. K. Nørskov, The Challenge of Electrochemical Ammonia Synthesis: A New Perspective on the Role of Nitrogen Scaling Relations, *ChemSusChem*, 2015, **8**, 2180–2186.

57 Z. W. Seh, J. Kibsgaard, C. F. Dickens, I. Chorkendorff, J. K. Nørskov and T. F. Jaramillo, Combining Theory and Experiment in Electrocatalysis: Insights into Materials Design, *Science*, 2017, **355**, eaad4998.

58 S. Ji, Z. Wang and J.-X. Zhao, A Boron-Interstitial Doped C_2N Layer as a Metal-Free Electrocatalyst for N_2 Fixation: A Computational Study, *J. Mater. Chem. A*, 2019, **7**, 2392–2399.

59 C. Ling, X. Niu, Q. Li, A. Du and J. Wang, Metal-Free Single Atom Catalyst for N_2 Fixation Driven by Visible Light, *J. Am. Chem. Soc.*, 2018, **140**, 14161–14168.

60 E. Skulason, T. Bligaard, S. Gudmundsdóttir, F. Studt, J. Rossmeisl, F. Abild-Pedersen, T. Vegge, H. Jónsson and J. K. Nørskov, A Theoretical Evaluation of Possible Transition Metal Electro-Catalysts for N_2 Reduction, *Phys. Chem. Chem. Phys.*, 2012, **14**, 1235–1245.

61 S. Kuriyama, K. Arashiba, K. Nakajima, H. Tanaka, N. Kamaru, K. Yoshizawa and Y. Nishibayashi, Catalytic Formation of Ammonia from Molecular Dinitrogen by Use of Dinitrogen-Bridged Dimolybdenum–Dinitrogen Complexes Bearing PNP-Pincer Ligands: Remarkable Effect of Substituent at PNP-Pincer Ligand, *J. Am. Chem. Soc.*, 2014, **136**, 9719–9731.

62 M.-A. Légaré, G. Bélanger-Chabot, R. D. Dewhurst, E. Welz, I. Krummenacher, B. Engels and H. Braunschweig, Nitrogen Fixation and Reduction at Boron, *Science*, 2018, **359**, 896–900.

63 R. Lan, J. T. Irvine and S. Tao, Synthesis of Ammonia Directly from Air and Water at Ambient Temperature and Pressure, *Sci. Rep.*, 2013, **3**, 1145.

64 S. Licht, B. Cui, B. Wang, F.-F. Li, J. Lau and S. Liu, Ammonia Synthesis by N_2 and Steam Electrolysis in Molten Hydroxide Suspensions of Nanoscale Fe_2O_3, *Science*, 2014, **345**, 637–640.

65 V. Kordali, G. Kyriacou and C. Lambrou, Electrochemical Synthesis of Ammonia at Atmospheric Pressure and Low Temperature in a Solid Polymer Electrolyte Cell, *Chem. Commun.*, 2000, 1673–1674.

66 D. Bao, Q. Zhang, F. L. Meng, H. X. Zhong, M. M. Shi, Y. Zhang, J. M. Yan, Q. Jiang and X. B. Zhang, Electrochemical Reduction of N_2 under Ambient Conditions for Artificial N_2 Fixation and Renewable Energy Storage Using N_2/NH_3 Cycle, *Adv. Mater.*, 2017, **29**, 1604799.

67 L. Zhang, S. M. Sharada, A. R. Singh, B. A. Rohr, Y. Su, L. Qiao and J. K. Nørskov, A Theoretical Study of the Effect of a Non-Aqueous Proton Donor on Electrochemical Ammonia Synthesis, *Phys. Chem. Chem. Phys.*, 2018, **20**, 4982–4989.

68 A. R. Singh, B. A. Rohr, J. A. Schwalbe, M. Cargnello, K. Chan, T. F. Jaramillo, I. Chorkendorff and J. K. Nørskov, Electrochemical Ammonia Synthesis—the Selectivity Challenge, *ACS Catal.*, 2017, **7**, 706–709.

69 Z. Chen, X. Zhang and G. Lu, Overpotential for CO_2 Electroreduction Lowered on Strained Penta-Twinned Cu Nanowires, *Chem. Sci.*, 2015, **6**, 6829–6835.

70 Y. Luo, G.-F. Chen, L. Ding, X. Chen, L.-X. Ding and H. Wang, Efficient Electrocatalytic N_2 Fixation with MXene under Ambient Conditions, *Joule*, 2019, **3**, 279–289.

71 H. K. Lee, C. S. L. Koh, Y. H. Lee, C. Liu, I. Y. Phang, X. Han, C.-K. Tsung and X. Y. Ling, Favoring the Unfavored: Selective Electrochemical Nitrogen Fixation Using a Reticular Chemistry Approach, *Sci. Adv.*, 2018, **4**, eaar3208.

72 J. Greeley, T. F. Jaramillo, J. Bonde, I. Chorkendorff and J. K. Nørskov, Computational High-Throughput Screening of Electrocatalytic Materials for Hydrogen Evolution, in *Materials for Sustainable Energy: A Collection of Peer-Reviewed Research and Review Articles from Nature Publishing Group*, World Scientific, 2011, pp. 280–284.

73 J. K. Nørskov, T. Bligaard, A. Logadottir, J. Kitchin, J. G. Chen, S. Pandelov and U. Stimming, Trends in the Exchange Current for Hydrogen Evolution, *J. Electrochem. Soc.*, 2005, **152**, J23–J26.